

Hydrodynamic Assembly of Astrocyte Cells in Conductive Hollow Microfibers

Lionel J. Ouedraogo, Mychal J. Trznadel, McKayla Kling, Vahid Nasirian, Alexandra G. Borst, Mehran Abbasi Shirsavar, Andrew Makowski, Marilyn C. McNamara, Reza Montazami,* and Nicole N. Hashemi*


The manufacturing of 3D cell scaffoldings provides advantages for modeling diseases and injuries as it enables the creation of physiologically relevant platforms. A triple-flow microfluidic device is developed to rapidly fabricate alginate/graphene hollow microfibers based on the gelation of alginate induced with CaCl_2 . This five-channel microdevice actualizes continuous mild fabrication of hollow fibers under an optimized flow rate ratio of 300:200:100 $\mu\text{L min}^{-1}$. The polymer solution is 2.5% alginate in 0.1% graphene and a 30% polyethylene glycol solution is used as the sheath and core solutions. The biocompatibility of these conductive microfibers by encapsulating mouse astrocyte cells (C8D1A) within the scaffolds is investigated. The cells can successfully survive both the manufacturing process and prolonged encapsulation for up to 8 days, where there is between 18–53% of live cells on both the alginate microfibers and alginate/graphene microfibers. These unique 3D hollow scaffolds can significantly enhance the available surface area for nutrient transport to the cells. In addition, these conductive hollow scaffolds illustrate unique advantages such as 0.728 $\text{cm}^3 \text{gr}^{-1}$ porosity and two times more electrical conductivity in comparison to alginate scaffolds. The results confirm the potential of these scaffolds as a microenvironment that supports cell growth.

1. Introduction

Tissue engineering has been used to make large strides in the development of native tissues used for maintenance of tissue, repair or regeneration of damaged tissues, and the study of cell–cell interactions based on engineering and biological principles.^[1] In the field of tissue engineering, cellular activities, scaffolds, and growth factors are the primary foci.^[2,3] Most microstructure scaffolds used for tissue assembly possess a broad range of advantages such as desired geometry, biocompatibility, biodegradability, ideal porosity, and desired mechanical properties.^[3–14] Microstructure scaffolds have been fabricated through various techniques such as phase separation, particulate leaching, microfluidics, hydrogels, rapid prototyping, electrospinning, and self-assembly.^[15–17]

Alginate 3D hydrogels are one of the most efficient microstructure scaffolds for a multitude of reasons and are used in many impressive, growing areas in biomedical engineering including, therapy, drug delivery, filtration, channeling, and target delivery of small volumes of liquid to live organisms.^[18–21] The Alginate 3D hydrogel can efficiently hold a large volume of water inside its porous cross-linked network, which is crucial for developing the extracellular matrix during cell encapsulation.^[22–26] The patterns of the fibers fabricated by the Alginate 3D hydrogels and their considerable surface-to-volume ratio are more attractive than other alginate hydrogel patterns because they have similar physiological properties to those of fiber proteins, including the ability to efficiently mimic continuous nutrient addition and metabolite removal like what is done in native tissue.^[27–29] Compared to pure alginate fibers,^[30] alginate/graphene fibers allow much rougher and more porous structures, which in turn provide more surface area while utilizing an equivalent volume. The Alginate 3D hydrogel is approved by the Food and Drug Administration (FDA), can be obtained from brown seaweed making it cost-effective and convenient, and the hollow alginate microfibers made from the hydrogel have desired geometries and mechanical properties.^[23,26,31–35]

L. J. Ouedraogo, M. J. Trznadel, M. Kling, V. Nasirian, A. G. Borst, M. A. Shirsavar, A. Makowski, M. C. McNamara, R. Montazami, N. N. Hashemi
Department of Mechanical Engineering
Iowa State University
Ames, IA 50011, USA
E-mail: reza@iastate.edu; nastaran@iastate.edu
M. Kling, A. G. Borst, N. N. Hashemi
Neuroscience Graduate Program
Iowa State University
Ames, IA 50011, USA

 The ORCID identification number(s) for the author(s) of this article can be found under <https://doi.org/10.1002/adbi.202300455>

© 2023 The Authors. Advanced Biology published by Wiley-VCH GmbH. This is an open access article under the terms of the Creative Commons Attribution-NonCommercial-NoDerivs License, which permits use and distribution in any medium, provided the original work is properly cited, the use is non-commercial and no modifications or adaptations are made.

DOI: 10.1002/adbi.202300455

Ideal conditions can be achieved by adjusting the flow rate ratios (FRRs) between the fluid core and sheath flows. Microfluidic hollow microfibers have the potential to be used in various ways such as for tissue engineering, in cell bioreactors, and for biopharmaceutical purification.^[23,31,36–40]

Recently, the induction of electrical properties to hydrogel structures by conductive biocompatible modifiers such as graphene, graphene oxide, reduced graphene oxide, and synthetic polymers such as polypyrrole or poly(3,4-ethylenedioxythiophene) polystyrene sulfonate (PEDOT:PSS) have been investigated by a number of studies to elucidate electrical cell-to-cell communication mechanisms within neuronal cell cultures.^[13,41–50] With the recent use of conductive biocompatible modifiers, alginate 3D microstructures have the potential to be further improved to accommodate the use of electrical stimulation on specific cell cultures and experiments. Specifically, the implementation of conductive biocompatible modifiers to alginate 3D microstructures may lead to more accurate and elaborate neuronal cell cultures where electrical stimuli are much more prevalent. Additionally, the increased conductivity of the fibers in relation to the addition of graphene may lead to advancements in other applications. One such application includes real-time cell sensing. The encapsulation of cells and a conductive material, such as graphene, can result in electrical sensors being able to accurately monitor the position of cells at specific times due to the heightened conductance that is linked to the cells.^[41] While the use of conductive biocompatible modifiers may also have implications for a variety of cell research, it is important to note that the main impact of these modifiers relates to improvements to the practices around neuronal cells. Graphene is an ideal conductive substance because it has a two-dimensional honeycomb structure of sp^2 hybridized carbons, outstanding biocompatibility, high conductivity, and remarkable mechanical properties.^[43,51–55] Graphene is highly flexible and stable under the harshest biological environments, allowing it to aid in the longevity of biological engineering and cellular growth, unlike other conductive substances such as polyesters and polypyrrole.^[53] Compared to graphene oxide, graphene that has not been oxidized produces less *in vivo* toxicity, in other words, apoptosis.^[52,56] However, it does require additional mechanical and electrical equipment or toxic surfactants to reduce the interfacial interactions between its carbonic layers before it can be used in cell-encapsulated hydrogels.^[52,57–59] It has been found that non-aggregated aqueous graphene dispersion with high stability can be obtained using a mechanical method in which the graphite is stirred in the presence of water-soluble bovine serum albumin (BSA).^[52,60–62] This method is a suitable alternative for thermal or chemical reduction of graphene oxide and does not require extensive use of cytotoxic chemicals to maintain the aqueous graphene dispersions.^[52]

Alginate hydrogels have been used to encapsulate astrocytes and alginate/graphene hydrogels have been used to encapsulate dopaminergic neuronal cells; however, to our knowledge, these are the first experiments done that involve encapsulating astrocytes in alginate/graphene microfibers. The conductive hydrogels have the potential to be a highly responsive scaffold for *in vitro* cell growth, drug delivery, and tissue regeneration. Biosensors based on conductive hydrogels have also been developed and put to use. One of the main applications of conductive hol-

low microfibers could be in modeling and mimicking the microvasculature systems in the body, such as the blood–brain barrier. Since the blood–brain barrier consists of capillary endothelial cells, basement membrane, neuroglial membrane, and glial podocytes, like astrocyte cells,^[63] the addition of graphene as a conductivity modifier seems vital to both communications between neural cells and regulation of the structure and function of the blood–brain barrier. To further improve the conductivity of the fibrous scaffolds, biocompatible hydrogels loaded with graphene may be used, potentially creating a real-time sensing platform for electrically based cell-to-cell communication. It is possible to produce graphene-alginate microfibers in a microfluidic system, which would allow for the encapsulation of mouse astrocyte cells within conductive 3D tissue scaffolding, allowing for the generation of real-time 3D sensor arrays with high physiological relevance. The conductivity of alginate microfibers can be greatly improved through the use of graphene without compromising the microfibers' capacity to support long-term cell survival. The fabrication and characterization of these astrocyte-encapsulating alginate/graphene microfibers and the study of the viability of the astrocytes during prolonged encapsulation are the focus of these experiments. This article also discusses the potential use of such biocompatible hydrogel platforms for the survival, regeneration, and electrical stimulation of human nervous system cells.

2. Experimental Section

2.1. Materials

Dulbecco's modified Eagle's medium (DMEM) and penicillin-streptomycin (Pen/Strep) solution (penicillin 10 000 U mL⁻¹/streptomycin 10 000 µg mL⁻¹, 15140-122, 100 mL) were purchased from Gibco Laboratories (Gibco Life Technologies Limited, Paisley, UK) and Gibco Life Technologies, respectively. Fetal bovine serum (FBS) (Qualified One Shot, Ref#: A31606-01, 50 mL) and Triton X-100 were from Thermo Fisher Scientific (Waltham, MA). Six-well cell culture clusters (Lot# 23 314 037) were purchased from Costar. Polyethylene glycol (PEG) (Mn = 20 000), Graphite (Synthetic graphite powder < 20 µm), paraformaldehyde, and BSA (A7906) were purchased from Sigma-Aldrich (St. Louis, MO). The low-viscosity sodium alginate was from Alfa Aesar (Ward Hill, MA, USA). CaCl₂·2H₂O was from Fisher Chemical, Waltham, MA, USA. The aqueous solutions were sterilized using a 3 µm pore size polytetrafluoroethylene (PTFE) syringe filter (Tisch Scientific, North Bend, OH, USA), followed by a 0.45 µm pore size polyvinylidene difluoride (PVDF) syringe filter (Fisherbrand, Houston, TX, USA). For all experiments, the ultrapure water (18.2 MΩ cm) was prepared by the Thermo Fisher Scientific water system (Waltham, MA). All other chemicals used were of AR grades and were used without further purification.

2.2. Instruments

A JCM-6000 NeoScope Benchtop scanning electron microscope (SEM, JEOL Ltd, Japan) at 15 kV acceleration voltage with a secondary electron detector was used to study the morphology of

air-dried microfibers. A Zeiss Axio Observer Z1 Inverted Microscope (Carl Zeiss, Oberkochen, Germany) was used to capture fluorescent images. Image processing was carried out with AxioVision Special Edition 64-bit software. The electrical behaviors of the hollow microfibers were determined by Electrochemical Impedance Spectroscopy (EIS), Cyclic Voltammetry (CV), Galvanostatic Charge–Discharge (GCD), and through the use of a Potentiostat system (Versa STAT 4, Princeton Applied Research, Princeton, USA). Three GenieTouch syringe pumps (Kent Scientific Corporation) were used to inject solutions. A 4-axis computerized numerical control (CNC) USB controller Mk3/4 for a mini CNC mill was used to mill the five-channel microfluidic device controlled by PlanetCNC (Ljubljana, Slovenia).

2.3. Fabrication of Microfluidic Devices

The microfluidic devices used in this study were fabricated from 6.0 mm thickness poly (methyl methacrylate) (PMMA, Grainger, IL, US) using a (CNC) mini-mill (Minitech Machinery Corporation, Norcross, GA). The core channels and the chevrons were milled with the dimensions of 1.00 mm × 0.75 mm (width × height) and 0.375 mm × 0.25 mm (width × height), respectively. Specifically, the channels were designed to allow for a hollow microfiber to be produced through a cross-linking solution solidifying only the core and sheath solution. Additionally, the channel dimensions were manufactured to limit the outer diameter of the microfibers to a maximum of 1.00 mm.^[64] The two faces of the PMMA chip were milled separately and then bonded together using solvent-assisted thermal bonding. To successfully bind the two faces of the PMMA chip, each face was first cleaned to remove any dust. Next, one face was placed in a vacuum oven at 74 °C and covered with ethanol. The second face was then aligned and placed on top of the preceding face with pressure being applied.^[64] The employed AlTiN-coated end mill cutters and drill bits were purchased from Harvey Tools and Grainger.

2.4. Preparation of Soluble Graphene Samples Through Ball Milling Process

Aqueous BSA-graphene was used to enhance the electrical conductivity of the pre-hydrogel solution. The few-layer graphene (FLG) was fabricated through liquid-phase exfoliation of graphite crystallites, ≈20 μm in size. To do this, an aqueous mixture containing 20.00 mg mL⁻¹ graphite and 2.00 mg mL⁻¹ BSA was prepared in plastic containers sealed with glue before placing them in metal containers. Steel balls with a diameter of 11/32" and 1/2" were used to apply shear tensions at 300 rpm rotational speed. The ratio of the balls' surface area to the solution volume for all solutions was constant at 500 ± 10 m² m⁻³. The exfoliation process was carried out for 90 h.

2.5. Cell Culture

A solution containing 45.0 mL DMEM maintenance media, 5.0 mL FBS, and 0.5 mL penicillin (10 000 U mL⁻¹)-streptomycin (10 000 μg mL⁻¹) was used to culture C8D1A astrocytes in T-25

flasks maintained at 37 °C under 5% CO₂ atmosphere. After 70% confluency, these cells were passaged three times before the encapsulation procedure. Trypsin solution (2 mL) was added, and then 1000.0 μL of the obtained cell suspension was added to the 3.0 mL alginate/graphene dispersion. C8D1A cells were cultured for five days in vitro to provide sufficient time to grow and proliferate within a 3D hydrogel alginate/graphene hollow microfiber.

2.6. Preparation of Solutions

During our experiments, we found that a 2.5% alginate solution containing 0.1% BSA-graphene had an ideal viscosity to resist shear force within the microfluidic channel and fabricate smoother alginate/graphene hollow microfibers. Most importantly, these experiments were used to determine the proper chemical composition of solutions that would create an ideal environment for cells to live. Specifically, the compositions that were used focused on forming a porous fiber structure that would allow cellular nutrients and waste to diffuse in and out of the fibers.^[30] Hence, 0.25 g sodium alginate powder (Alfa Aesar, Ward Hill, MA) was sterilized with 70% ethanol under a UV lamp and dissolved in 8.0 mL of WFI-Quality Cell Culture grade water (Corning, Corning, NY). Then, 1.0 mL of freshly mixed, UV-sterilized 0.01 g L⁻¹ BSA-graphene dispersion was added to the solution mentioned above, and stirring was continued. This obtained polymer solution was mixed with 1.0 mL of cell suspension (3.1725 × 10⁶ cells mL⁻¹). 30% PEG (Aldrich Chemistry, St. Louis, MO), whose dispersing solvent is DI water, was used for the sheath and core solutions. A sterilized 30.0% CaCl₂·2H₂O solution was used for the collection bath.

2.7. Microfluidic Manufacturing of Alginate/Graphene Hollow Microfiber

The five-channel microfluidic device and all other items used were first carefully wiped with a tissue containing 70% ethanol and irradiated by UV under a laminar flow hood to ensure sterile conditions during the experiments. The 2.5% alginate sodium solution containing 0.1 % graphene was mixed with 3.1725 × 10⁶ C8D1A cells/mL in a sterilized Falcon 15 mL conical centrifuge tube. The resulting mixture was placed into two 3.0 mL BD syringes to connect the microfluidic device's two side polymer channels. Subsequently, the core and sheath solutions (30% w/v PEG) were connected to the center channel and the other two side channels to guide and solidify the polymer solution. This dispersion of the PEG polymer was chosen because it has high biocompatibility with many cells and is therefore used extensively in tissue engineering with no significant side effects on cells. A core: polymer (cladding): sheath FRR of 300:200:100 (μL min⁻¹) rate was applied to the microfluidic channels. This polymeric mixture was introduced to a 30% CaCl₂·2H₂O collection bath upon exiting the microfluidic device. As a result of the cross-linking procedure between alginate carboxylate groups, the alginate/graphene hollow microfibers become solidified in the presence of Ca²⁺ which causes further enhancement of their strength.^[23,65] PEG, on the other hand, does not polymerize in the presence of Ca²⁺ so it simply runs off into

FBS-DMEM media to suspend the hollow fibers and maintain their sample humidity during imaging.

2.11. Cell Viability

A solution containing Green-CMFD and PI was used to study the viability of C8D1A cells and to investigate the 3D environment's long-term biocompatibility and potential for C8D1A proliferation and differentiation. Previous studies have shown that the addition of graphene did not change the long-term cell viability; however, contact with graphene might alter the gene expression of cells.^[41] PI was a common fluorescent counterstain of nuclei and chromosomes used to identify membrane damage in dead cells.^[67] CMFDA could freely pass through cell membranes and react with live cellular components. During these reactions, CMFDA was converted to cell-impairment products, which could pass to daughter cells through several generations without transferring to other cells in the population. The C8D1A cells were studied for 8 days to study their viability through prolonged encapsulation in the alginate/graphene hollow microfibers.

2.12. Porosity and Electrochemical Behavior

Fiber porosity was determined by conducting a Brunauer-Emmett-Teller (BET) analysis. During the analysis, a sample was exposed to a known amount of nitrogen gas. After the nitrogen gas was exposed to the sample, the amount of gas was measured again. Depending on the porosity of the sample, varying amounts of nitrogen gas would be adsorbed. A more porous sample would adsorb more gas due to the increased surface area. Thus, less returning gas would be measured. A less porous sample would adsorb less gas, and thus have a lower surface area.

The electrochemical performance of prepared alginate/graphene hollow microfibers was studied by CV using an electrode constructed from hollow microfibers and H_3PO_4 /PVA electrolyte. A voltage range of -0.1 to $+0.1$ V was used to record the data for both the alginate and alginate/graphene fibers. In addition, differing current densities were applied to each of the fibers to determine the differences in capacitance between each fiber composition.

2.13. Statistical Analysis

Statistical analysis was carried out with R Project Statistical Software to conduct an Analysis of Variance (ANOVA) to compare the means of the cell viability data across samples. Cell viability data for this experiment was calculated by taking the number of live cells divided by the total number of cells in a microfiber obtained from a live-dead cell assay. An average from all of the microfibers was calculated for days 1–8 of the experiment post-manufacturing. These means were compared between the pure alginate group and the alginate/graphene group.

2.14. Flow Rate Experiments

Flow rate experiments were conducted to determine an optimal inner and outer diameter for the fibers. Specifically, experiments

were conducted to determine the effects of higher flow rate ratios compared to lower flow rate ratios. During the experiments, fibers created using both the higher and lower flow rate ratios were tested. Through the experiments, it was concluded that higher flow rate ratios led to a thinner outer fiber wall with lower flow rate ratios forming a thicker outer fiber wall.

2.15. SEM Imaging

Imaging was conducted by using a JCM-6000 NeoScope Benchtop scanning electron microscope. Fibers were mounted on paper frames and placed into the microscope using carbon NEM tape. Images for the different fibers were then able to be collected.

3. Results

This study investigated the polymerization of alginate solution with the addition of aqueous BSA-graphene dispersion within the microfluidic device. Several physical properties of the hollow fibers were obtained by investigating the following parameters: FRR, morphology, size, porosity, electrochemical performance determined by CV, capacitance, density, and nitrogen adsorption. The optimized microfluidic parameters, optimized flow rates for the polymer, sheath, and core solutions and their effect on bond strength and cross-linking density formed between the alginate's functional groups, and the cell viability of the encapsulated astrocytes were also investigated.

3.1. Flow Rate Ratio

The effect of the influence of flow rate ratio on the geometries of alginate/graphene hollow microfibers was evaluated. Diameters of alginate/graphene hollow microfibers under different flow rate ratios are shown in **Figure 2c,d**. As seen in **Figure 2**, the inner diameter of the hollow microfibers is smaller at a lower flow rate ratio than a higher flow rate ratio, while the outer diameter stays fairly consistent at both low and high flow rate ratios. The thickness of the hollow microfiber is determined by the difference between the size of the inner diameter and outer diameter. The smaller the inner diameter, the thicker the hollow microfiber. It was determined that lower flow rate ratios allow for the fabrication of larger hollow microfibers due to an enhanced hydrodynamic focusing (a technique that gives users the ability to gauge the size of particles in a flow channel) applied on the core fluid by the polymer and sheath fluids that lead to loss of inner diameter.^[68] Specifically, hydrodynamic focusing functions by manipulating the cross-sectional area of the flow in the microfluidic channel. For instance, two fluids that have an equal flow running next to each other in the channel will occupy an equivalent area. By increasing the flow rate of one of these fluids, the area that is occupied by that corresponding fluid will increase, while the area occupied by the other fluid will decrease. In the case of this experiment, the inner and outer diameters were able to be manipulated by varying the flow rates of the different solutions and thus altering the respective areas.^[69]

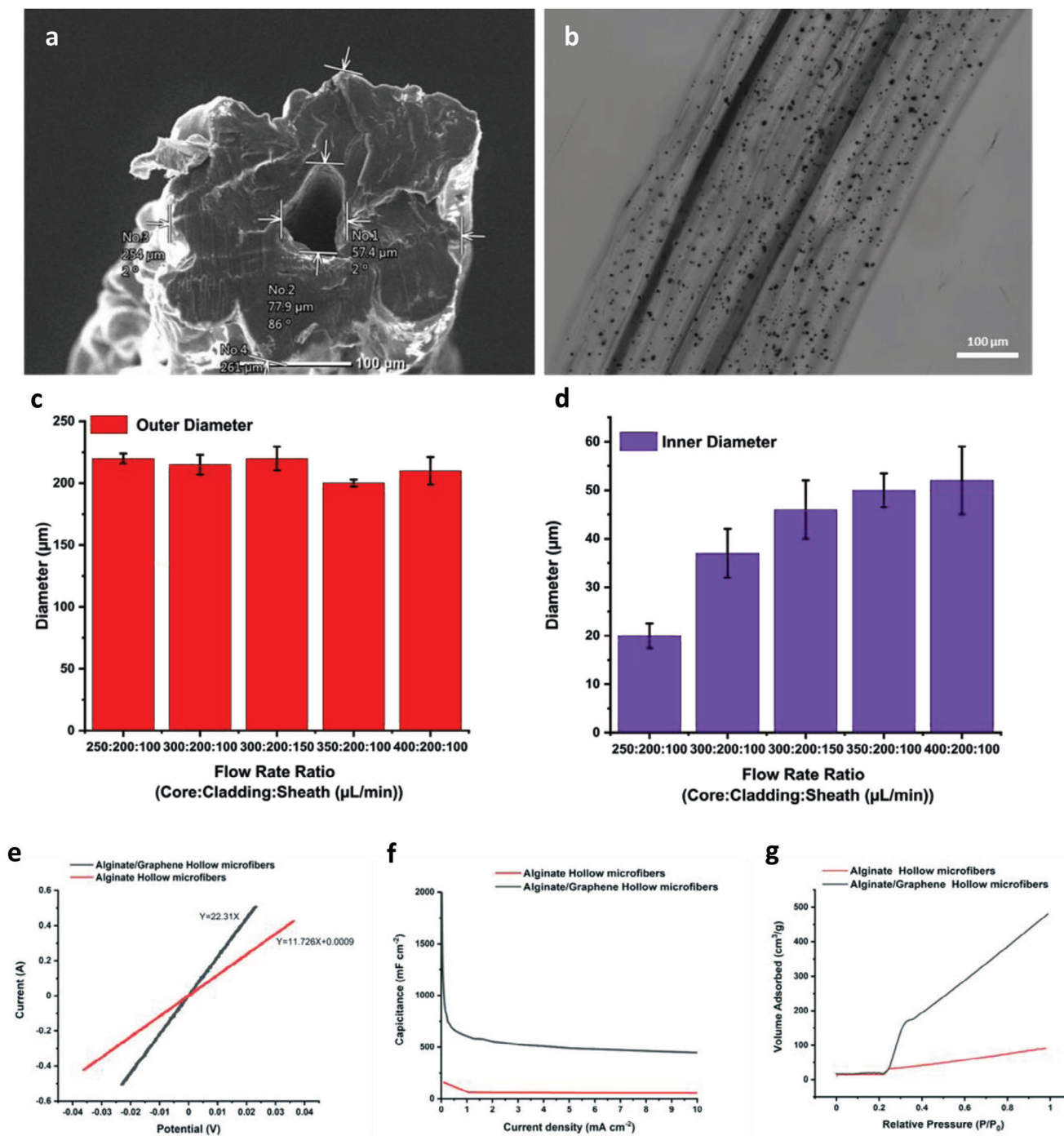


Figure 2. a) SEM analysis of microfluidic alginate/graphene hollow microfibers manufactured under optimized parameters. All microfibers had a wall thickness of $\approx 70\text{--}90\ \mu\text{m}$ with lumen diameters of $\approx 50\ \mu\text{m}$. As can be seen in the image, this particular microfiber has inner diameters of $77.9\ \mu\text{m}$ (No 2) and $57.4\ \mu\text{m}$ (No 1). No 3 and No 4 are the outer diameters of the microfiber being $254\ \mu\text{m}$ (No 3) and $261\ \mu\text{m}$ (No 4). With these diameters, the wall thickness is $\approx 88\ \mu\text{m}$. b) Illustrative environmental optical microscope image of the alginate/graphene hollow microfibers prepared in this study. c) The effect of flow rate ratio on the outer diameter of alginate/graphene hollow microfibers prepared by the five-channel microfluidic device. d) The effect of flow rate ratio on the inner diameter of alginate/graphene hollow microfibers prepared by the five-channel microfluidic device. e) CV curves of alginate and alginate/graphene hollow microfibers at a scan rate of $100.0\ \text{mV s}^{-1}$. f) The capacitances of alginate and alginate/graphene hollow microfibers under different current densities. g) The inset is the typical nitrogen adsorption of hollow microfibers. The volume of nitrogen adsorbed is greater in alginate/graphene hollow microfibers than in alginate hollow microfibers.

3.2. Morphology

The microscopic morphology of alginate/graphene hollow microfibers was studied by SEM and their overall dimensions were determined. Figure 2a displays a cross-sectional SEM image of a manufactured conductive microfluidic hollow microfiber. As the figure shows, the surface of the alginate/graphene hollow microfiber surface has a high roughness. The roughness may be a result of the turbulence that occurs when BSA-graphene is introduced to the alginate solution. In other words, both the core and outer layer of alginate/graphene hollow microfibers display a porous manner along the entirety of the structure. The average inner diameter of the hollow microfibers was found to be $\approx 50.0 \mu\text{m}$ and the average outer diameter of the microfibers was $\approx 200.0 \mu\text{m}$, as shown in Figure 2. Microfibers of this size were fabricated using optimized microfluidic parameters, which were determined to be a 2.5% (w/v) alginate concentration containing 0.1% (w/v) BSA-graphene. Figure 2b shows an optical microscope image of the hollow microfibers fabricated with the optimized flow rates for the polymer, sheath, and core solutions, which were 200, 100, and 350 $\mu\text{L min}^{-1}$, respectively. The average diameters of the fibers were used to optimize the specific flow rates used in the experiment with each average being linked to a corresponding flow rate. Due to the outer diameters of each flow rate, depicted in Figure 3, having a dimension of $\approx 200.0 \mu\text{m}$, the optimized flow rate will also need to form an outer diameter of 200.0 μm to ensure that the variance between diameters due to flow rates is reduced. By applying this principle to the inner diameter, the optimal flow rate is able to be determined. Since the average inner diameter of the fibers is 50.0 μm , a flow rate that forms a 50 μm diameter will be used as the optimal flow rate. Thus, a flow rate of 350:200:100 $\mu\text{L min}^{-1}$ was able to satisfy the parameters set by the average diameters of the fiber. Figure 2 as a whole also confirms the intermediate duct that is present along the length of the alginate/graphene hollow microfibers and shows that it has minimal changes in its thickness.

3.3. Porosity and Electrochemical Behavior

The CV results obtained were recorded in the voltage range of -0.1 – $+0.1$ V and are shown in Figure 2e. The CV curves of prepared alginate/graphene hollow microfibers display a linear behavior. Figure 2f displays discharge curves including the specific capacitance and density of alginate and alginate/graphene hollow microfibers. At the current density range of 0.0–10.0 mA cm^{-2} , alginate/graphene hollow microfibers expressed larger specific capacitances than pure hollow alginate microfibers. The capacitance of the alginate/graphene microfibers is ≈ 500 – 600 mF cm^{-2} , while the capacitance of the alginate microfibers is $\approx 50 \text{ mF cm}^{-2}$. Also, of note, the alginate/graphene hollow microfibers maintained the ability to preserve their substantial capacitance when the current density was increased to 10.0 mA cm^{-2} . As expected from the alginate/graphene microfibers having a higher capacitance than the alginate microfibers, a better conductivity with a symmetric shape was achieved in alginate/graphene hollow microfibers compared to the pure alginate samples.

The porosity of alginate/graphene and alginate microfibers was studied and successfully confirmed by N_2 adsorption isotherm measurement (Figure 2g). A higher level of N_2 adsorption indicates greater porosity in the material whereas a lower level of N_2 indicates less porosity in the material. As seen in Figure 2g, the total pore volume (TPV) of the alginate/graphene hollow microfiber surface was calculated to be $0.728 \text{ cm}^3 \text{ g}^{-1}$, using the following equation:

$$\text{TPV} = Q_{\text{sat}} \times (P_{\text{vap}}/P_{\text{liq}}) \quad (1)$$

where Q_{sat} is the N_2 adsorption quantity, P_{vap} is the density of N_2 vapor at STP (1.2504 gL^{-1}), and P_{liq} is the density of liquid N_2 at its boiling point (807 gL^{-1}). Compared to a pure alginate hollow microfiber with a TPV of $\approx 0.139 \text{ cm}^3 \text{ g}^{-1}$, the alginate/graphene hollow microstructure maintained a considerably larger N_2 volume due to many pores on the alginate/graphene hollow microfiber surface present after the addition of graphene.

3.4. Cell Viability

Figure 3a–h shows the fluorescent microscopy images related to cell viability taken during 8 days following fabrication of alginate/graphene hollow microfibers with astrocytes encapsulated. As seen, the encapsulated astrocyte cells inside the hollow microfibers showed a high survival rate of 94% during the microfluidic fabrication process (Figure 3a₁). The lowest cell viability in the alginate/graphene microfibers was seen on day 5, which was 83%. The alginate control group was also evaluated for cell viability (Figure 3i–k). The alginate control group had a 99.3% survival rate measured immediately after fabrication (Figure 3i). The lowest cell viability in the alginate microfibers was measured to be 86.5% on day 3. Statistical analysis was performed to see if there were any significant differences in cell viability between the two groups. Based on the obtained results, the alginate group had a significantly higher mean of live cells on day 1, immediately after manufacturing (Figure 3l).

3.5. Electrical Stimulation

Electrical stimulation experiments were performed to determine the effects the addition of graphene would have on the conductivity of the hollow microfibers. The input of 1 V that was used, stemmed from a study that determined a voltage of mV per mm was sufficient to induce cell proliferation for rat olfactory cells.^[70] This idea, along with the conclusion that the diameter of the fibers was to be no > 100 micrometers, was used to calculate the optimal voltage of 1 V. Since mouse astrocytes were embedded within the microfibers, it was reasonable that an effective voltage for the rat cells would also apply to mouse cells due to similarities between the species. The additional voltages studied served as controls to show contrasts between the effects on the cells embedded within each fiber. Several precautions were taken into consideration to ensure that the cells within the fibers were not contaminated or affected by any ionization during the procedure. To accomplish this goal, salt bridges, which are generally used to reduce the effects of ionization that commonly occurs between metal wires and cell media, were created.

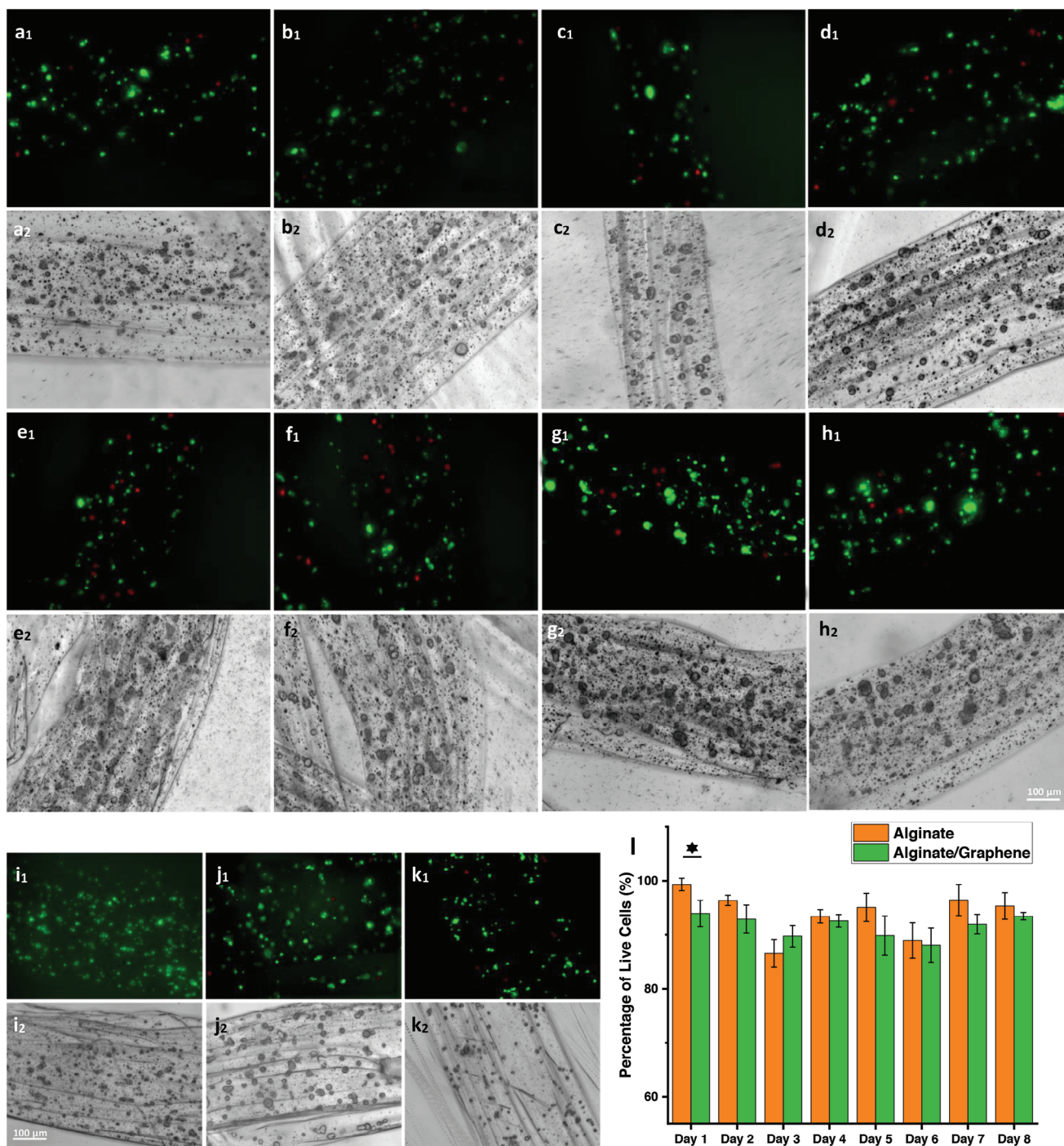


Figure 3. A live-dead cell assay of 2.5% alginate/0.1% graphene hollow microfibers with C8D1A cells encapsulated within. These microfibers were created with a core and sheath of 30% PEG and a FRR of 200:300:100 $\mu\text{L min}^{-1}$: $\mu\text{L min}^{-1}$: $\mu\text{L min}^{-1}$. Samples were gathered in a collection bath of 30% $\text{CaCl}_2 \cdot 2\text{H}_2\text{O}$. This live-dead cell assay contains Cell Tracker CMFDA and PI. Live cells are shown with the CMFDA in green and dead cells are shown with the PI in red. Live-dead cell assays were performed on days 1–8. a_1 – h_1 are fluorescent images of the live-dead cell assays on days 1–8. a_2 – h_2 are brightfield images of the same frames as a_1 – h_1 . Based on these images, alginate/graphene hollow microfibers show the ability to maintain cell viability of astrocytes after encapsulation for eight days. ($i_{1,2}$ – $k_{1,2}$) A control group live-dead cell assay of 2.5% alginate microfibers with C8D1A cells encapsulated within the hollow microfibers. This live-dead cell assay contains Cell Tracker CMFDA (green, live cells) and PI (red, dead cells) and was performed on days 1–8. i_1 – k_1 shows fluorescent images of encapsulated astrocytes showing high cell viability rates. a_2 – k_2 are brightfield images of the same frames as i_1 – k_1 . i_1 and i_2 are on day 1, j_1 and j_2 are on day 5, and k_1 and k_2 are on day 8. l) Graph of cell viability data showing days versus percentage of live cells in both the alginate control group and the alginate/graphene group on all 8 days. This graph shows that both the alginate control group and alginate/graphene group have high cell viability rates. Alginate was found to have higher cell viability every day except for day 3. The only day that showed statistically significant differences in cell viability was day 1. For statistical analysis, ANOVA was performed; $*p < 0.05$ was used for statistical significance.

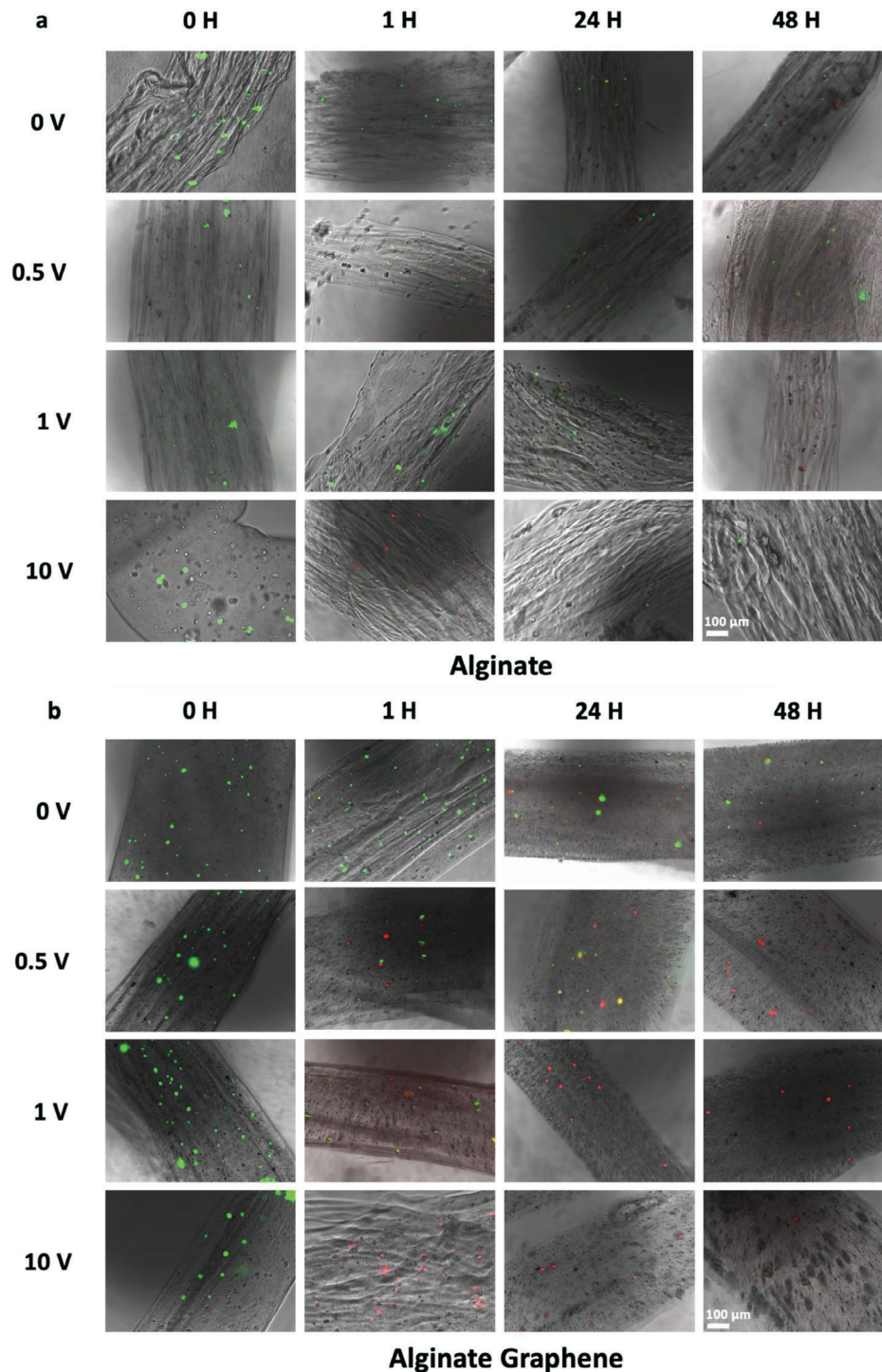


Figure 4. a) SEM analysis of alginate microfibers that were exposed to varying voltages. At 0 h, there was zero voltage applied for all samples reflecting a control. The green dye indicates cells that are alive, while the red dye indicates cells that are dead. b) SEM analysis of alginate/graphene microfibers that followed the same treatments as the alginate microfibers. Scale bar: 100 µm.

Data for collection times up to 48 h can be seen below in **Figure 4**. It was concluded that times beyond 48 h would be unnecessary due to relevant data trends being observed prior to this point. After 48 h, no new data trends were observed and the cells were 100% dead, meaning no live cells were on either the alginate mi-

crofibers or alginate/graphene microfibers. As seen in **Figure 4a**, the embedded mouse astrocytes continued to live to varying degrees until data collection was stopped at the 48-h mark. At a voltage of 10 V, 62.5% of cells were shown to have died at 24 h, which reflects using a voltage that was 10 times the optimal voltage of

1 V. Additionally, voltages of 0 V and 500 mV resulted in the cells being shown to be alive up to the conclusion of data collection. The fibers exposed to the 500 mV were shown to have fewer dead cells at the 24-h mark, 22.2% dead, and the 48-h mark, 46.2% dead, when compared to other voltages including 0 V, 40% dead at 24-h mark, and 47.6% dead at 48-h mark. This may suggest that the optimal exposure voltage for cell proliferation is closer to 500 mV for the mouse astrocytes compared to the 1 V used for reference with the rat olfactory cells. Furthermore, as seen in Figure 4a, 80% of the cells were shown to have died at 48 h at 1 V of exposure, but 50% of the cells lived at 10 V of exposure. However, it is worth noting that 94.9% of the cells died immediately after being exposed to 10 V, as seen at the 1-h mark, while 83.3% of cells lived immediately after being exposed to 1 V, as seen at the 1-h mark. As a result, 94.9% of cells had previously died at 10 V, which left few living cells within the corresponding fibers for the remainder of the experiment. In contrast, 83.3% of cells exposed to 1 V started to die sometime after 24 h since 60% of the cells were shown to be alive at 24 h but only 28.6% of cells were alive at 48 h. Based on this information, while the fibers exposed to a voltage of 1 V at the 48-h mark were shown to have more dead cells, specifically 71.4% dead, the fibers exposed to a voltage of 1 V were primarily composed of recently deceased cells since 31.4% of the living cells at the 24-h mark died by the 48-h mark. On the other hand, while there was a greater quantity of living cells, specifically 50% alive cells, at the 48-h mark in the fibers exposed to 10 V, there were significantly fewer total cells compared to the number of recently deceased cells in the fiber exposed to 1 V. This implies that the living cells in the fiber exposed to 10 V may be an outlier due to the vast majority of cells that died much earlier at the same voltage.

On the other hand, as seen in Figure 4b, the embedded mouse astrocytes are shown to die after 1 h for every voltage except 0 V to differing degrees. The vast majority of cells were shown to be dead, starting at the 24-h mark where 1 V had 94.12% dead cells and 10 V had 100% dead cells, respectively. In addition, the fibers exposed to a voltage of 500 mV at 24 h had a ratio that was approximately one-to-one with respect to living cells and dead cells. This means $\approx 50\%$ of cells were alive and 50% of cells were dead. Similarly, a voltage of 10 V was shown to have immediate effects on the state of the cells, with the cells dying shortly after the electrical stimulation. Based on this information, the fibers that were formed using graphene had a much lower resistance to electricity as reflected by the death of cells at the 1-h mark with a voltage of 500 mV compared to the death of cells in the alginate fibers primarily existing at a voltage of 1 V and 10 V once 48 h had passed. Since the same set of voltages were applied to both the alginate and alginate/graphene microfibers, it was determined that the addition of graphene to the microfibers led to an increase in conductivity. This increased conductivity caused a voltage that would be safe for cells within the alginate fiber but unsafe for cells within the alginate/graphene fiber. As a result, it can be determined that the addition of graphene permits a lower input voltage to be applied to the fibers since the resistance of the fibers is lower. A lower possible voltage mimics the levels of electrical signals that exist in organisms closer, which further contributes to the similarities with organic structures that the hollow microfibers are attempting to reach.

4. Discussion

The physical properties of the microfibers, the optimized microfluidic parameters and flow rates, and the cell viability of the astrocytes, all of which were investigated in this study, gave insight into an ideal method for fabrication of alginate/graphene hollow microfibers with encapsulated astrocytes, the ways in which alginate/graphene microfibers could be deemed superior to pure alginate fibers, and the potential uses of these microfibers.

An important characteristic of the alginate/graphene hollow microfibers is their ability to perform effective ion transport throughout the electrode, which was confirmed by the CV curves of the prepared alginate/graphene microfibers displaying a linear behavior. Another important feature of the alginate/graphene microfibers is their ability to support the entrance of nutrients through the inner cavity as well as the removal of waste. This is ensured through the dissolving of the PEG once the microfiber is dispensed into the $\text{CaCl}_2 \cdot 2\text{H}_2\text{O}$ bath. When the alginate/graphene solution polymerizes and the PEG solution does not, the latter runs off into the water bath leaving a hollow channel that forms inside the shell of the alginate/graphene structure that now has astrocytes encapsulated in the walls. The hollow channel provides a pathway for nutrients, and other necessary agents for the survival of the astrocyte cells, to enter the interior of the structure.

We also found that at the current densities used in our experiments, 0.0–10.0 mA cm^{-2} , the alginate/graphene microfibers expressed a much higher specific capacitance than the pure alginate microfibers. In materials with 3D networks of particles such as porous graphene or carbon monoliths, their hierarchical porosity comes from the connectivity of the macropores and micropores.^[71] If there is good contact between the particles in their alignment in the 3D network, the materials will have a high electrical conductivity. Both hierarchical porosity and high electrical conductivity contribute to a material being a supercapacitor.^[72] The porous graphene used in this experiment is a structure composed of sheets with hierarchical pores just like what is discussed above.^[73] As shown in Figure 2f, the capacitance of the alginate/graphene microfibers is $\approx 500\text{--}600 \text{ mF cm}^{-2}$, while the capacitance of the alginate microfibers is $\approx 50 \text{ mF cm}^{-2}$. Increased porosity is commonly linked to higher values of capacitance because of the additional ion transportation pathways that are formed as a result of a heightened amount of porosity. Specifically, the increased porosity of the alginate/graphene microfibers leads to the creation of active ion adsorption sites which also causes an increase in capacitance.^[74] This shows that alginate/graphene microfibers have a much higher capacitance than the alginate microfibers supporting the idea that the alginate/graphene microfibers have a hierarchical porous network that lends itself to high electrical conductivity and supercapacitance while their counterpart does not, making the alginate/graphene microfibers better suited for use for the encapsulation of astrocytes. The porous network in the alginate/graphene microfibers is also important for allowing media and nutrients to permeate efficiently through the alginate/graphene wall. The transfer of nutrients and metabolic waste must be considered if these scaffolds are to be used for cell culture inside their lumen. In the future, the mechanism of the

formation of the porous network in the alginate/graphene microfibers should be determined as it is not yet known. The idea is that it is either achieved through the alginate-Ca-alginate linkages creating a mesoporous structure in the walls of the microfluidic alginate/graphene hollow microfibers or through hydrophilic behaviors present in the microfibers. Which of these are true has yet to be determined.

Incorporating graphene as a conductive modifier yields microfiber samples with enhanced ion diffusion because of the material's increased porosity and ion-carrying channels. Hollow alginate/graphene microfibers, due to the addition of graphene, can show more advantage in charge-discharge operations than hollow alginate fibers by virtue of their larger peak current, longer discharging duration, and lack of obvious ohmic loss at the low current densities. The fast movement of electrons within this mesoporous structure is made conceivable by the enormous effective surface area, which provides adequate electrical double-layer capacitance as ion-accessible route channels. Enhanced electrochemical performance was the final outcome of these continuous ion transport networks.^[74]

The encapsulation of astrocyte cells within alginate/graphene hollow microfibers using a microfluidic platform is proving to be an effective strategy for the development of biomaterial-based therapeutics and drug delivery systems that can be used hereafter. Overall, the introduction of graphene to the alginate microfiber did not impede cell viability with the exception of day one immediately after exposure to graphene. This method is much more cell-friendly and more cytocompatibility than other methods that exist like electrospinning,^[75] which must be operated under high voltage to achieve polymerization. In this method, there is no need for post-processing^[76] after fibers are fabricated because the astrocytes are already encapsulated, which reduces the overall manufacturing time and complexity. This high throughput method is also proving to be successful as far as the cell viability of the astrocytes encapsulated in the wall of alginate/graphene microfibers goes. Hence, this approach for cell delivery via a hydrogel pathway could improve cell-cell interactions and its feasibility for in vitro cell culture and regenerative medicine.

5. Conclusion

We have developed a tunable alginate/graphene hollow microfiber-based microfluidic platform for long-term support of in vitro culture of encapsulated C8D1A cells. C8D1A cells were encapsulated in alginate/graphene hollow microfibers as a proof of concept to show that these cells could survive and proliferate in the fabricated microenvironment. By introducing BSA-graphene into hollow alginate microfibers, their conductivities were enhanced to scalable intracellular recording and stimulation of neuronal cells. In this study, the addition of 0.1% graphene to the alginate microfibers led to an improvement in conductivity by a factor of two. The present findings display the first description of the ability of porous, conductive, hollow alginate/graphene microfibers to maintain high cell viability while addressing some of the disadvantages of alginate hydrogels in terms of electrical characteristics. We propose further developing this microfluidic technique to achieve a controlled cell number on alginate/graphene hollow microfibers' inner and

outer surfaces for applications such as cellular therapies, and drug- and gene-delivery strategies.

Acknowledgements

L.J.O., M.J.T., and M.K. contributed equally to this work. This work was partially supported by the Office of Naval Research Grant N000141712620 and National Science Foundation Awards 2321975 and 2014346. The authors would like to thank Nima Alimoradi for his assistance with the illustration, and Wenyu Huang and Puranjan Chatterjee for their helpful insights into porosity characterizations.

Open access funding provided by the Iowa State University Library.

Conflict of Interest

The authors declare no conflict of interest.

Data Availability Statement

The data that support the findings of this study are available from the corresponding author upon reasonable request.

Keywords

astrocytes, biomanufacturing, composite microstructures, conductive microfibers, microfluidics, neural tissue engineering

Received: August 28, 2023

Revised: October 19, 2023

Published online:

- [1] J. P. Vacanti, C. A. Vacanti, in *Principles of tissue engineering*, 4th ed, Elsevier, London **2014**, pp. 3–8.
- [2] N. G. Rim, C. S. Shin, H. Shin, *Biomed. Mater.* **2013**, *8*, 014102.
- [3] A. Khademhosseini, R. Langer, J. Borenstein, J. P. Vacanti, *Proc. Natl. Acad. Sci. USA* **2006**, *103*, 2480.
- [4] S. L. Tao, T. A. Desai, *Adv. Drug Delivery Rev.* **2003**, *55*, 315.
- [5] K. Y. Suh, A. Khademhosseini, P. J. Yoo, R. Langer, *Biomed. Microdevices* **2004**, *6*, 223.
- [6] W. Nijdam, J. d. Jong, C. J. M. v. Rijn, T. Visser, L. Versteeg, G. Kapantaidakis, G.-H. Koops, M. Wessling, *J. Membr. Sci.* **2005**, *256*, 209.
- [7] Z. Bai, J. M. Mendoza Reyes, R. Montazami, N. Hashemi, *J. Mater. Chem. A* **2014**, *2*, 4878.
- [8] S. Sirivisoot, R. Pareta, B. S. Harrison, *3DInterface Focus* **2014**, *4*, 20130050.
- [9] D. Mawad, A. Artzy-Schnirman, J. Tonkin, J. Ramos, S. Inal, M. M. Mahat, N. Darwish, L. Zwi-Dantsis, G. G. Malliaras, J. J. Gooding, *Chem. Mater.* **2016**, *28*, 6080.
- [10] S. Inal, A. Hama, M. Ferro, C. Pitsalidis, J. Oziat, D. Iandolo, A.-M. Pappa, M. Hadida, M. Huerta, D. Marchat, P. Mailley, R. M. Owens, *Adv. Biosyst.* **2017**, *1*, 1700052.
- [11] S. Wang, S. Guan, J. Xu, W. Li, D. Ge, C. Sun, T. Liu, X. Ma, *Biomater. Sci.* **2017**, *5*, 2024.
- [12] B. Niemczyk, P. Sajkiewicz, D. Kolbuk, *J. Neural Eng.* **2018**, *15*, 051002.
- [13] E. D. Osipova, Y. K. Komleva, A. V. Morgun, O. L. Lopatina, Y. A. Panina, R. Y. Olovyannikova, E. F. Vais, V. V. Salmin, A. B. Salmina, *Front. Aging Neurosci.* **2018**, *10*, 234.

- [14] Q. Zhang, S. Beirne, K. Shu, D. Esrafilzadeh, X.-F. Huang, G. G. Wallace, *Sci. Rep.* **2018**, *8*, 13461.
- [15] J. L. Drury, D. J. Mooney, *Biomaterials* **2003**, *24*, 4337.
- [16] S. M. Peltola, F. P. W. Melchels, D. W. Grijpma, M. Kellomäki, *Ann. Med.* **2008**, *40*, 268.
- [17] R. Murugan, S. Ramakrishna, *Tissue Eng.* **2006**, *12*, 435.
- [18] N. A. Peppas, J. Z. Hilt, A. Khademhosseini, R. Langer, *Adv. Mater.* **2006**, *18*, 1345.
- [19] A. D. Augst, H. J. Kong, D. J. Mooney, *Macromol. Biosci.* **2006**, *6*, 623.
- [20] A. Singh, N. A. Peppas, *Adv. Mater.* **2014**, *26*, 6530.
- [21] W. Gombotz, *Adv. Drug Delivery Rev.* **1998**, *31*, 267.
- [22] Z.-J. Meng, W. Wang, R. Xie, X.-J. Ju, Z. Liu, L.-Y. Chu, *Lab Chip* **2016**, *16*, 2673.
- [23] M. C. Mcnamara, F. Sharifi, J. Okuzono, R. Montazami, N. N. Hashemi, *ACS Appl Bio Mater* **2019**, *2*, 1603.
- [24] E. Amici, G. Tetradis-Meris, C. P. De Torres, F. Jousse, *Food Hydrocolloids* **2008**, *22*, 97.
- [25] V. Liu Tsang, S. N. Bhatia, *Adv. Drug Delivery Rev.* **2004**, *56*, 1635.
- [26] S. M. Yoo, R. Ghosh, *J. Membr. Sci.* **2018**, *558*, 45.
- [27] C. P. Barnes, S. A. Sell, E. D. Boland, D. G. Simpson, G. L. Bowlin, *Adv. Drug Delivery Rev.* **2007**, *59*, 1413.
- [28] U. Marx, H. Matthes, A. Nagel, R. Baehr, *Am. biotech. lab.* **1993**, *11*, 26.
- [29] A. Ouyang, S.-T. Yang, *Expert Opin. Biol. Ther.* **2008**, *8*, 895.
- [30] M. C. McNamara, A. E. Niaraki-Asli, J. Guo, J. Okuzono, R. Montazami, N. N. Hashemi, *Front. Mater.* **2020**, *7*, 61.
- [31] M. C. McNamara, F. Sharifi, A. H. Wrede, D. F. Kimlinger, D.-G. Thomas, J. B. Vander Wiel, Y. Chen, R. Montazami, N. N. Hashemi, *Macromol. Biosci.* **2017**, *17*, 1700279.
- [32] H. Onoe, S. Takeuchi, *Drug Discovery Today* **2015**, *20*, 236.
- [33] J. Zhang, Z. Wang, M. Liu, F. Zhao, Z. Wu, *J. Membr. Sci.* **2017**, *526*, 272.
- [34] M. J. Ellis, J. B. Chaudhuri, *Biotechnol. Bioeng.* **2007**, *96*, 177.
- [35] S. S. Aykar, N. Alimoradi, M. Taghavimehr, R. Montazami, N. N. Hashemi, *Adv. Healthcare Mater.* **2022**, *11*, 2102701.
- [36] D. Sechi, B. Greer, J. Johnson, N. Hashemi, *Anal. Chem.* **2013**, *85*, 10733.
- [37] N. Hashemi, J. M. Lackore, F. Sharifi, P. J. Goodrich, M. L. Winchell, N. Hashemi, *Technology* **2016**, *4*, 98.
- [38] R. L. Pemathilaka, J. D. Caplin, S. S. Aykar, R. Montazami, N. N. Hashemi, *Glob. Chall.* **2019**, *3*, 1800112.
- [39] T. Andersen, P. Auk-Emblem, M. Dornish, *Microarrays* **2015**, *4*, 133.
- [40] A. Bozza, *Alginate-Based Hydrogels for Central Nervous System Tissue Regeneration*, University of Trento, Trento **2015**.
- [41] Y. Bu, H.-X. Xu, X. Li, W.-J. Xu, Y. Yin, H. Dai, X. Wang, Z.-J. Huang, P.-H. Xu, *RSC Adv.* **2018**, *8*, 10806.
- [42] C. Heo, J. Yoo, S. Lee, A. Jo, S. Jung, H. Yoo, Y. H. Lee, M. Suh, *Biomaterials* **2011**, *32*, 19.
- [43] N. Thayumanavan, P. Tambe, G. Joshi, M. Shukla, *Compos. Interfaces* **2014**, *21*, 487.
- [44] X. Liu, A. L. Miller li, S. Park, B. E. Waletzki, A. Terzic, M. J. Yaszemski, L. Lu, *J. Mater. Chem. B* **2016**, *4*, 6930.
- [45] X. Liu, A. L. Miller, S. Park, B. E. Waletzki, Z. Zhou, A. Terzic, L. Lu, *ACS Appl. Mater. Interfaces* **2017**, *9*, 14677.
- [46] A. E. Niaraki Asli, J. Guo, P. L. Lai, R. Montazami, N. N. Hashemi, *Biosensors* **2020**, *10*, 6.
- [47] M. C. McNamara, S. S. Aykar, R. Montazami, N. N. Hashemi, *ACS Macro Lett.* **2021**, *10*, 732.
- [48] M. C. McNamara, S. S. Aykar, N. Alimoradi, A. E. Niaraki Asli, R. L. Pemathilaka, A. H. Wrede, R. Montazami, N. N. Hashemi, *Adv. Biol.* **2021**, *5*, 2101026.
- [49] A. Niaraki, M. C. McNamara, R. Montazami, N. N. Hashemi, *ACS Appl. Bio. Mater.* **2022**, *5*, 113.
- [50] H. Acar, S. Çinar, M. Thunga, M. R. Kessler, N. Hashemi, R. Montazami, *Adv. Funct. Mater.* **2014**, *24*, 4135.
- [51] L. Feng, Z. Liu, *Nanomedicine* **2011**, *6*, 317.
- [52] S. Ahadian, M. Estili, V. J. Surya, J. Ramón-Azcón, X. Liang, H. Shiku, M. Ramalingam, T. Matsue, Y. Sakka, H. Bae, K. Nakajima, Y. Kawazoe, A. Khademhosseini, *Nanoscale* **2015**, *7*, 6436.
- [53] G. Reina, J. M. González-Domínguez, A. Criado, E. Vázquez, A. Bianco, M. Prato, *Chem. Soc. Rev.* **2017**, *46*, 4400.
- [54] A. Karamati, N. Hunter, H. Lin, H. Zobeiri, S. Xu, X. Wang, *Int. J. Heat Mass Transfer* **2022**, *198*, 123393.
- [55] N. Hunter, A. Karamati, Y. Xie, H. Lin, X. Wang, *Chem. Phys. Chem.* **2022**, *23*, e202200417.
- [56] M. C. Duch, G. R. S. Budinger, Y. T. Liang, S. Soberanes, D. Urich, S. E. Chiarella, L. A. Campochiaro, A. Gonzalez, N. S. Chandel, M. C. Hersam, G. M. Mutlu, *Nano Lett.* **2011**, *11*, 5201.
- [57] A. González-Mayorga, E. López-Dolado, M. C. Gutiérrez, J. E. Collazos-Castro, M. L. Ferrer, F. Del Monte, M. C. Serrano, *ACS Omega* **2017**, *2*, 8253.
- [58] M. C. Serrano, M. J. Feito, A. González-Mayorga, R. Diez-Orejas, M. C. Matesanz, M. T. Portolés, *Biomater. Sci.* **2018**, *6*, 2987.
- [59] A. Ghanem, M. Abdel Rehim, *Biomedicines* **2018**, *6*, 63.
- [60] O. Gianak, E. Pavlidou, C. Sarafidis, V. Karageorgiou, E. Deliyanni, *Separations* **2018**, *5*, 25.
- [61] Z. Ismail, A. H. Abdullah, A. S. Zainal Abidin, K. Yusoh, *J. Nanostructure Chem.* **2017**, *7*, 231.
- [62] A. Pattammattel, C. V. Kumar, *Adv. Funct. Mater.* **2015**, *25*, 7088.
- [63] A. K. Dotiwala, C. McCausland, N. S. Samra, *Anatomy, Head and Neck, Blood-Brain Barrier*, **2018**.
- [64] S. S. Aykar, D. E. Reynolds, M. C. McNamara, N. N. Hashemi, *RSC Adv.* **2020**, *10*, 4095.
- [65] M. C. McNamara, R. J. Pretzer, R. Montazami, N. N. Hashemi, *Clean Technologies* **2019**, *1*, 265.
- [66] D. D. Kumar, *Alternate Forms of Salt Bridges*.
- [67] Z. Wang, T. Mizoguchi, T. Kuribara, M. Nakajima, M. Iwata, Y. Sakamoto, H. Nakamura, T. Murayama, T. Nemoto, M. Itoh, *Open Biol.* **2021**, *11*, 200241.
- [68] M. Lu, F. Sharifi, N. N. Hashemi, R. Montazami, *Macromol. Mater. Eng.* **2017**, *302*, 1600544.
- [69] J. P. Golden, G. A. Justin, M. Nasir, F. S. Ligler, *Anal. Bioanal. Chem.* **2012**, *402*, 325.
- [70] M. R. Love, S. Palee, S. C. Chattipakorn, N. Chattipakorn, *J. Cell. Physiol.* **2018**, *233*, 1860.
- [71] A. Garcia-Gomez, V. Barranco, G. Moreno-Fernandez, J. Ibañez, T. A. Centeno, J. M. Rojo, *J. Phys. Chem. C* **2014**, *118*, 5134.
- [72] M. Sethi, H. Bantawal, U. S. Shenoy, D. K. Bhat, *J. Alloys Compd.* **2019**, *799*, 256.
- [73] Y. W. Sun, W. Liu, I. Hernandez, J. Gonzalez, F. Rodriguez, D. J. Dunstan, C. J. Humphreys, *Phys. Rev. Lett.* **2019**, *123*, 135501.
- [74] V. Nasirian, A. E. Niaraki-Asli, S. S. Aykar, M. Taghavimehr, R. Montazami, N. N. Hashemi, *3D Printing and Additive Manufacturing* **2022**, <https://doi.org/10.1089/3dp.2022.0026>.
- [75] V. D. Ranjan, P. Zeng, B. Li, Y. Zhang, *Biomater. Sci.* **2020**, *8*, 2175.
- [76] E. Bosch-Rué, L. M. Delgado, F. J. Gil, R. A. Perez, *Biofabrication* **2020**, *13*, 015003.